J Mater Sci (2007) 42:4276–4290
DOI 10.1007/s10853-006-0619-1

Calorimetric studies of 8090 and 1441 Al–Li–Cu–Mg–Zr alloys of conventional and retrogressed and reaged tempers

K. S. Ghosh · K. Das · U. K. Chatterjee

Received: 17 November 2005 / Accepted: 26 June 2006 / Published online: 28 February 2007

Abstract The differential scanning calorimetry (DSC) technique has been used to examine the solid state reactions of GPB zones formation, precipitation of δ', T_1, T_2, S', δ phases and their dissolution occurring in the 8090 and 1441 Al–Li–Cu–Mg–Zr alloys of the water-quenched (WQ), peak aged T8 and T6, over aged T7, retrogressed (R), retrogressed and reaged (RRA) T77 tempers. All the exothermic and endothermic peaks in the DSC thermograms have been identified and discussed. The noticeable differences observed in the thermograms of the 8090 and 1441 alloys have been explained and this is attributed to the variation in the concentrations of the solute elements Li, Cu and Mg in the alloys. The peak temperatures as well as the heat evolved and absorbed during the precipitation and dissolution reactions have been determined with the help of the built-in software of the simultaneous thermal analyzer (STA) used for DSC studies. X-ray diffractograms and a few TEM micrographs have been illustrated to correlate the reactions in these alloys. Further, all the thermograms of the WQ state of the 1441 alloy, taken at four different heating rates, have exhibited overlapping peaks of GPB zones formation and the δ' phase precipitation. The overlapping peaks cause restrictions in determining the kinetic parameters of activation energy and growth parameter, but, interestingly, the thermograms of retrogressed tempers have showed separate peaks of GPB zones formation and δ' phase precipitation which will easily enable to find out kinetic parameters, by varying heating rate method.

K. S. Ghosh (✉)
Department of Metallurgical and Materials Engineering, National Institute of Technology, Warangal 506004, India
e-mail: ksghosh2001@yahoo.co.uk

K. Das · U. K. Chatterjee
Department of Metallurgical and Materials Engineering, Indian Institute of Technology, Kharagpur 721 302, India

Introduction

Al–Li alloys are of strategic important in aerospace vehicle design as these are characterized by higher Young's modulus, and lower density compared to other aluminium base alloys [1, 2]. But, Al–Li alloys have unattractive fracture behaviour, and especially poor ductility and toughness arising mainly due to the inhomogeneous nature of slip resulting from coherent matrix strengthening ordered δ' (Al_3Li) precipitates and the presence of coarse equilibrium δ (AlLi) precipitates at the grain boundaries [3–5]. However, in commercial pentanary Al–Li–Cu–Mg–Zr alloys, slip is homogenized by introducing (i) dispersoids of β' (Al_3Zr), with the addition of zirconium and, (ii) semicoherent/incoherent precipitates, such as T_1 (Al_2CuLi), θ' (Al_2Cu), or S (Al_2CuMg), through copper and magnesium additions. Thus, the commercial development of the Al–Li–Cu–Mg–Zr alloys has prompted investigations of the basic phase equilibria and transformations that can occur within this complex system. The large number of metastable precipitates and phases that occur in the alloy and the wide variety of aging treatments employed can lead to complex microstructural conditions [6–9].

Although transmission electron microscopy (TEM) is used for observation of microstructural features, but for a rapid and quantitative description of phase transformations, differential scanning calorimetry (DSC) [10–12] can notably be used as a supplement to (TEM) studies. Tedious and rigorous microstructural studies are required to confirm the existence of GPB zones formation at low temperature. However, DSC studies provide complimentary information at the low temperature phase transformation as well as in the high temperature phase fields of the system [13, 14]. In DSC technique, the dissolution peaks enable to detect, in particular, precipitated particles or zones even if their sizes are not large enough for an easy TEM characterization [15]. Further, precipitation and dissolution kinetic parameters can be easily obtained from the DSC thermograms.

The relatively new heat treatment process, namely retrogression and reaging (RRA), was originally developed to improve the combination of strength and resistance to stress corrosion cracking of the aluminium alloys 7075 [16, 17]. The RRA heat treatment process comprises heating the peak aged temper alloy for a very short time at an intermediate temperature, 200–240 °C (preferably above the matrix strengthening δ' solvus line) called retrogression and immediately reaging the retrogressed state to the peak aged temper. The total aging time in the RRA temper is twice than that of the aging time of the conventional peak aged temper. TEM studies of the changes in the microstructural features upon RRA treatment and the evolution of their most relevant properties, have been studied by many authors [18, 19]. In particular, a great deal of attention has been devoted to the study of the phase transformation promoted upon RRA treatments by TEM [20, 21]. However, literature is scanty on the evaluation of the microstructural alterations upon RRA treatment by DSC studies in the 8090 and 1441 alloys system. In the present paper, the authors have investigated the precipitation and dissolution reactions of the 8090 and 1441 Al–Li–Cu–Mg–Zr alloys in the various tempers such as solution treated and water quenched, peak aged T8 and T6, retrogressed (R), retrogressed and reaged (RRA) T77 and over aged T7 tempers in details by DSC technique and the results have been correlated with a few representative TEM micrographs and XRD studies.

Experimental techniques

Studies were carried out on the 8090 and 1441 (Russian grade) Al–Li–Cu–Mg–Zr alloys. The alloys were obtained in sheet form from the Defence Metallurgical Research Laboratory (DMRL), Hyderabad, India. The 8090 and 1441 alloys were cast, homogenized, hot rolled and cold rolled to the thickness of 2.8 and 2.0 mm, respectively. The cold rolled sheet of the 8090 alloy was solutionized at 530–535 °C, water quenched, stretched 1.5–2.5% followed by artificial aging at 170 °C for 24 h corresponding to the peak aged T8 temper. The cold rolled sheet of the 1441 alloy was solutionized at 530–535 °C, water quenched, stretched by 1.5–2.5%, followed by artificial aging at 150 °C for 4 h and then 170 °C for 24 h to the peak aged T8 temper. The chemical compositions (wt%) of the 8090 and 1441 alloys are given in Table 1.

The peak aged T8 temper alloys were subjected to retrogression and reaging (RRA) treatments. Retrogressions were carried out in a small vertical tube furnace in air and the furnace temperatures were maintained within ±2 °C of the set value. The samples of the peak aged temper were heated for a short duration at temperatures above and below the δ' solvus line of the Al–Li system, cooled in ice cold water followed by immediate reaging to various tempers. The retrogression treatments were carried out above the δ' solvus line of the alloy system [31], at four different temperatures [21]. Table 2 gives the RRA treatment schedules adapted to the 8090 and 1441 alloys for the DSC studies alone. For DSC studies, the selection of around 50 °C difference of retrogression temperature in these 8090 and 1441 alloys is based on the concept of the effect/phenomenon of faster dissolution kinetics with increasing temperatures. Prior to testing, solution treated and water quenched, the peak aged, retrogressed and RRA treated alloy sheet surfaces were ground to 100 μm minimum so as to remove the lithium and magnesium depleted zones and subsurface porosity zones developed during solutionizing the alloy which was carried out at temperature 530–535 °C in air [22].

DSC studies were carried out on both the alloys in their solutionized and water-quenched, conventional peak aged T8 and T6, retrogressed (R), retrogressed and under aged (RUA), retrogressed and isothermal and duplex peak aged (RRA) T77, and over aged T7

Table 1 Chemical compositions (in wt%) of the 8090 and 1441 Al–Li–Cu–Mg–Zr alloys

Alloy	Li	Cu	Mg	Zr	Fe	Si	Al
8090	2.29	1.24	0.82	0.12	0.09	0.044	Balance
1441	1.90	2.0	0.90	0.09	0.11	0.05	Balance

Table 2 Retrogression and reaging schedules adapted to the 8090 and 1441 alloys

Samples	Retrogression temperature and time	Reaging schedule	RRA temper designation
8090-T8	At 280 °C for 8 min	None	8090R280
1441-T8	At 230 °C for 15 min	None	1441R230
8090-T8	At 280 °C for 8 min	Isothermal reaging (IA) to peak aged temper i.e. at 170 °C for 24 h	8090R280IA
		Isothermal reaging to under aged temper i.e. at 170 °C for 2 h	8090R280UA
		Duplex aging (DA) at 150 °C for 36 h, followed by heating to 190 °C at a rate of 5–7 °C/min and holding for 1 h at the temperature	8090R280DA
1441-T8	At 230 °C for 15 min	Isothermal reaging (IA) to peak aged temper i.e. at 170 °C for 26 h	1441R230IA
		Isothermal reaging (IA) to under aged temper i.e. at 170 °C for 2 h	1441R230UA
		Duplex aging (DA) at 150 °C for 36 h, followed by heating to 190 °C at a rate of 5–7 °C/min and holding for 1 h at the temperature	1441R230DA

states. Specimens of approximately 30 mg were cut from the coupons of the various tempers of both the alloys. The sides of the specimens were made absolutely flat and smooth for very good contact with the crucible. DSC runs were performed using a Stanton Redcroft, Model STA 625 (heat flux type) simultaneous thermal analyzer. At least two runs were made for each sample in order to establish reproducibility.

DSC runs were carried out from ambient temperature and to around 500 °C at different heating rates in an ultra pure argon gas atmosphere. The STA system was purged with argon gas for half an hour before starting the experiment. A pure aluminium disc was used as the reference. The thermal analyzer was connected to a computer with a suitable interface; the data for each run was continuously stored. After a run was completed, the output i.e. the net heat flows as a function of temperature was recorded using the established calibration of the DSC cell. The baseline and sapphire data was used to generate a ''look-up'' table. During subsequent experiments this table was used to convert the raw data counts to rate of heat transfer.

For TEM studies, the samples were mechanically thinned to a thickness of approximately 100 μm, punched to get 3 mm disc and finally thinned down to perforation using a Fischione twin-jet electropolisher, operating at 25 V and 2.5 A current, in an electrolyte of composition 30% HNO_3 and 70% CH_3COOH at a temperature of approximately –20 °C. A Philips CM12 TEM was used for the observation of the microstructures. X-ray diffraction study was carried using a Philips PW 1710 diffractometer unit with cobalt and copper targets.

Results and discussion

DSC Thermograms of solution treated water quenched state

Figures 1 and 2 show the DSC thermograms of solution treated and water quenched 8090 and 1441 Al–Li–Cu–Mg–Zr alloys, respectively, at a heating rate of 10 °C/min. The curves are smoothened with the help of built-in software in the computer controlled DSC unit.

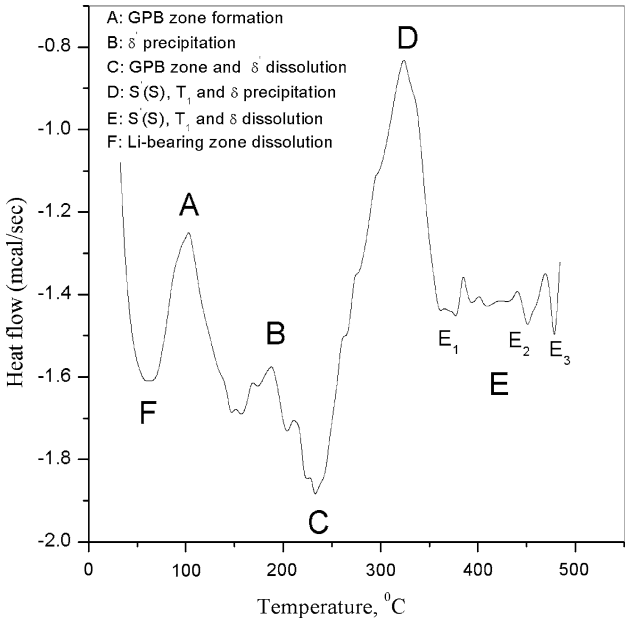

Fig. 1 DSC thermogram of solution treated and water quenched 8090 alloy at a heating rate of 10 °C/min

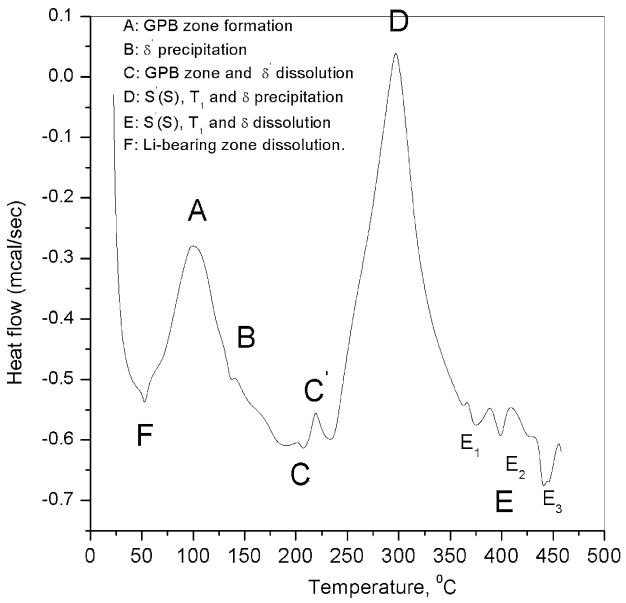

Fig. 2 DSC thermogram of solution treated and water quenched 1441 alloy at a heating rate of 10 °C/min

In the case of age hardenable aluminum alloys, normally the formation of precipitates is an exothermic process whilst their dissolution is an endothermic process [23]. The peak temperature for the precipitation represents the temperature at which the two factors i.e. the fall of the driving forces for the continued precipitation (i.e. the decrease of supersaturation with the rise of temperature during DSC run) and the increase of diffusivity with the increase of temperature compete and result in a maximum precipitation rate.

The thermograms (Figs. 1 and 2) exhibit many exothermic and endothermic peaks (marked with alphabets A–F) indicating the sequence of precipitation and dissolution reactions of the alloy system [23–29]. The first exothermic peak region A is attributed to the formation of GPB zones and peak region B is for the precipitation of δ' (Al_3Li) phase. Actually, GPB zone formation and precipitation of δ' commence from room temperature, so it is to be mentioned that the peak A is a compound and the same is also reported in literature [24]. Overlapping signals or fluctuations seen between peaks A and B, are due to the net effects of continued dissolution of GPB zones and the precipitation of δ' phase.

The peak region B in Fig. 2 for the 1441 alloy is not clearly resolved with a sharp peak, instead a small thermal fluctuation is observed. The alloy 1441 contains higher amounts of Cu and Mg compared to the 8090 alloy. The presence of Cu and Mg decreases Li solubility in Al alloys [30] which favours both the precipitation and growth of δ' particles, mostly in the first stages of aging. The δ' solvus line of the 1441 alloy is of the order of 20 °C lower than the δ' solvus line of the 8090 alloy, as estimated from the Al–Li phase diagram [31]. Further, it is to be mentioned that the excess solutes (which enhances the Li diffusivity) have an influence on the formation of δ' phase, but the coarsening of the δ' phase is not influenced by the excess solutes, instead it is assisted by the dislocations [28]. Thus, all these factors cause δ' precipitation in the 1441 alloy at a lower temperature, compared to the same in the 8090 alloy, with the result of overlapping of peak region B with the peak region A.

Due to the overlapping of the GPB zones formation and δ' precipitation, it is very difficult to determine the kinetic parameters of the phases by the varying heating rate method. But, the DSC thermograms of the retrogressed states show no such overlapping of the peaks for the GPB zones formation and δ' phase precipitation, instead peaks associated with these phases have formed separately which enables easily to determine kinetic parameters. DSC studies for the retrogressed and retrogressed and reaged tempers are discussed in details in section ''DSC thermograms of T8, retrogressed (R), RRA and T7 tempers''.

The endothermic peak region C is attributed to the dissolution of both GPB zones and δ' precipitates. The thermal fluctuation or, in other word, the existence of doublet is seen in the peak region C. Peak broadening or plateau near peak C could be attributed to dissolution of δ' phase with short range order and dissolution of fully ordered δ', as stated by Nozato and Nakai [32]. Balmuth [33] has mentioned that the dissolution temperature range reflects a range of particle sizes. Further, the existence of the doublets cannot be interpreted in terms of a single reaction but must, instead, be considered as the result of the superposition of the dissolution of δ' phase and the onset of the precipitation of the S′ (Al_2CuMg) and T_1 (Al_2CuLi) phases at the dislocation sites in the grains. The thermal fluctuation in the peak region C, might also reflect that the dissolution of δ' precipitate is delayed by the presence of β' (Al_3Zr) dispersoids i.e. especially the δ' particles which have precipitated on β' dispersoids or partially engulfed by the β' particles. Figure 3a, b, TEM photomicrographs i.e. the dark filed image of the δ' precipitates for the 8090-T8 and 8090R280IA tempers, respectively. The Fig. 3a, b also exhibits the duplex precipitates i.e. δ' precipitates coated on the β' (marked with arrow in the figure). Similar complex/duplex coated precipitates are observed and reported in literature [34]. The formation of duplex δ' (i.e., δ' coated β') particles is attributed to the fact that the presence of coherent β' dispersoids in the solid solution

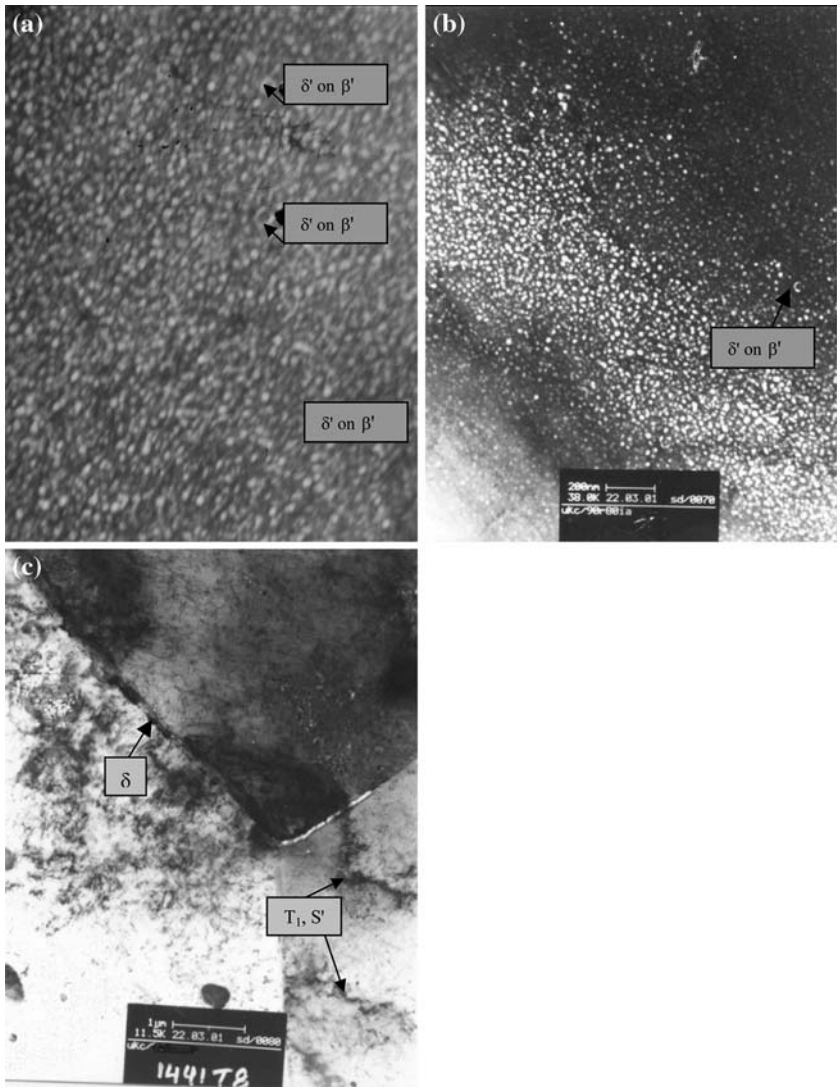

Fig. 3 TEM dark field image of δ' particles of (**a**) T8, (**b**) 8090R280IA RRA temper of the 8090 alloy and (**c**) TEM micrograph of the T8 temper of the 1441 alloy exhibits heterogeneous (preferentially along the dislocations) precipitation of S′ (Al_2CuMg), T_1 (Al_2CuLi) phases and equilibrium δ (AlLi) phase along the grain boundaries

acts an effective heterogeneous nucleation sites for the δ' precipitation owing to the reduction of both strain and surface energy. In fact, β' particles can induce δ' precipitation at lithium levels which are inadequate for homogeneous nucleation. The δ' precipitates coated on the β' will not dissolve easily [23], instead require higher thermal energy for the dissolution and hence the thermal fluctuation in the peak region C.

In Fig. 2 for the 1441 alloy, the thermal fluctuation and in fact, the existence of a distinct exothermic peak C′, is observed in the peak region C. Similar observation has also been reported in literature for Al–Li as well as in other Al base alloys [15]. This exothermic peak, C′ is the net effect of commencement of some precipitation reactions and the endothermic continued dissolution process of δ' precipitates within this temperature range. The appearance of exothermic C′ peak in the peak region C indicates exothermic precipitation reactions have dominated over the dissolution reactions of δ'. The exothermic reaction is considered to the heterogeneous precipitation of the S′ and T_1 phases (as observed in Fig. 3c), at the defects and dislocations (developed during quenching) and along the grain boundaries, as nucleation of these phases at the defects sites require much lower thermal energy. Furthermore, S′, may nucleate on δ' precipitates, as reported in Al–Li–Cu–Mg–Zr alloy [35]. But at this low temperature range homogeneous precipitation of T_1 and S′ precipitations will not occur, as homogeneous precipitation of T_1 and S′ phases requires much higher thermal energy. Thus, with the levels of supersaturations with solutes Cu, Mg and Li, the precipitations T_1 and S′ phases are not completed in the temperature range of peak region C. The thermogram shows that the heat flow occurs in the endothermic direction, indicating dominancy of the dissolution process, which is nothing but the ongoing

continued dissolution of the δ' precipitates, especially which are larger in size, pinned and engulfed with β' dispersoids [23].

Due to the appearance of C′ peak in the δ' phase dissolution range, it is very difficult to determine the kinetic parameters of the δ' phase dissolution accurately. However, the DSC thermograms of the retrogressed and RRA tempers do not show the formation of C′ peak which will enable to determine kinetic parameters accurately.

Peak region D is attributed to the formation of S′ (Al_2CuMg), T_1 (Al_2CuLi), T_2 (Al_6CuLi_3) and δ (AlLi) phases [15, 23, 24, 28, 36]. The S′ phase mostly precipitates homogeneously and heterogeneously in the matrix [6, 7, 21]. The T_1 and T_2 phases precipitate in the matrix as well as at the grain boundaries, where as the δ phase forms invariably at the grain and subgrain boundaries [6, 7, 21, 36]. The S′ phase is a strained version of the S phase. Therefore, the heat effects associated with the S′ → S transformation will be minimal, and in the DSC thermogram this transformation will not be exhibited separately [24]. The heat effects (Tables 3 and 4) associated with the peak D is quite large compared to that of the peak A and B together and this might be confirming that peak D represents the precipitation of S′ (S), T_1, T_2 and δ phases and the similar explanation is also stated in literature [24]. TEM studies of all these probable phases in the T8 and the microstructural alterations upon RRA treatment of the 8090 alloy have been discussed by the author [21] in detail.

The DSC peak region E exhibits a series of dissolution peaks and they are associated with the dissolution of S′ (S), T_1, T_2 and δ phases [24]. Meticulous studies are required to identify the individual dissolution peak in this region corresponding to the particular phase, and no literature is available regarding the identification of these dissolution peaks.

Calorimetric [37], high resolution phase-contrast imaging electron microscopy (HREM) [38], small-angle X-ray scattering (SAXS), small angle neutron scattering (SANS) [39, 40], and theoretical studies [41] in the Al–Li alloys reveal a cascade of phase transformation prior to δ' precipitation and the disordered solid solution undergoes congruent order to a transient non-stoichiometric ordered single-phase state. The congruent ordered state decomposes by secondary spinodal separation into regions lean of lithium and regions rich in lithium. Both regions are ordered at this stage but diffusion of lithium from lean to rich areas causes the former to disorder and later to evolve into stoichiometric $L1_2$ ordered domains. The final microstructure is then ordered δ' particles in a disordered matrix.

The appearance of an endothermic peak F at low temperature, in some of the DSC thermograms (Figs. 1 and 2), represent the dissolution of the Li-bearing zones i.e. the Li-lean regions, or even ordered Li-rich regions that still had to develop onto stoichiometric δ' (Al_3Li) composition [37, 41]. Noble and Trowsdale [37] believed, based on the evidences considered, it was caused by dissolution of subcritical $L1_2$ ordered

Table 3 Heat effects associated with the DSC peaks of solution treated and water quenched 8090 alloy at different heating rates

Alloy	Heating rate (°C/min)	Peak A		Peak B		Peak C		Peak D		Peak E		Peak F	
		H	T_p	H	T_p	H	T_p	H	T_p	H	T_p	H	T_p
8090	2.5	–1.94	78	–0.019	162	1.2	222	–3.95	282	5.8	354, 455, 479, 503	–	47
	5.0	–1.71	86	–0.037	187	1.1	228	–4.05	298	5.27	360, 454, 481, 508	0.46	53
	10	–1.07	91	–0.18	193	1.54	231	–3.98	306	5.15	363, 460, 486	0.58	59
	20	–1.15	112	–0.28	213	1.16	245	–4.06	341	3.95	415, 452, 479, 508	0.54	73

Table 4 Heat effects associated with the DSC peaks of solution treated and water quenched 1441 alloy at different heating rates

Alloy	Heating rate (°C/min)	Peak A		Peak B		Peak C		Peak D		Peak E		Peak E		Peak F	
		H	T_p	H	T_p	H	T_p	H	T_p	H	T_p	H	T_p	H	T_p
1441	2.5	–1.95	80	–	–	0.4	197	–3.03	260	–	–	–	34	–	37
	5.0	–1.92	84	–	–	0.6	205	–2.81	285	–	453, 480, 504	0.56	47	0.34	46
	10	–1.75	97	–	–	1.4	197, 220	–2.69	292	–	454, 478	0.72	52	0.50	52
	20	–0.67	113	–	–	2.18	180, 246	–3.39	319, 331	2.92	445	0.34	73	0.42	75

Where H is the evolution or absorption of heat in mcal/mol, T_p is the peak temperature, °C. Peak regions are: A—GPB zones formation; B—δ' precipitation zones; C—GPB and δ' dissolution; D—S′ (S), T_1, T_2 and δ precipitation; E—dissolution of S′ (S), T_1, T_2 and δ phases

regions. Sato et al. [38] and Lendvai et al. [42] invoked similar interpretation to explain the observed low temperature endotherm in their DSC studies of as-quenched Al–Li alloys. Further, Rio et al. [43] detected the formation of ordered regions of size less that 1 nm in Al–10 at% Li alloy, aged at 24 h at room temperature, by positron annihilation technique. They reported that these regions dissolved on heating after which growth of δ' was observed.

DSC Thermograms at varying heating rates

Figures 4 and 5 show the DSC curves of solution treated and water quenched 8090 and 1441 Al–Li–Cu–Mg–Zr alloys, respectively, at the heating rates of 2.5, 5, 10 and 20 °C/min. The sequence of exothermic and endothermic reactions marked as A–F peak regions, are observed in all the DSC curves of the varying heating rates. The identifications of the peaks have been discussed in the previous sections.

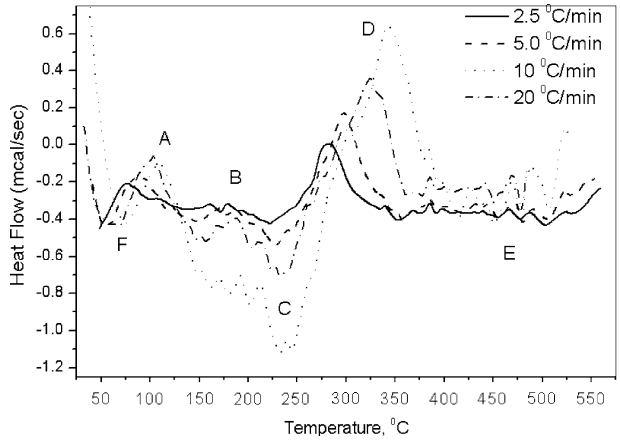

Fig. 4 DSC thermogram of solution treated and water quenched 8090 alloy at different heating rates. Table 3 gives the heat effects and peak temperature of the various peaks

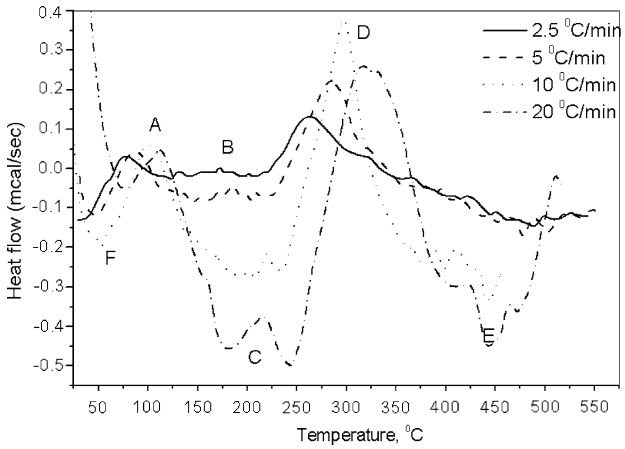

Fig. 5 DSC thermogram of solution treated and water quenched 1441 alloy at different heating rates. Table 4 gives the heat effects and peak temperature of the various peaks

The heat effects and the peak temperatures (T_p) associated with different precipitation and dissolution reactions as reflected in the thermograms for the 8090 and 1441 alloys in the solution treated and water quenched alloys are given in Tables 3 and 4, respectively. For the precipitation process, as the temperature rises the driving force for continued precipitation (i.e. the supersaturation) falls but the diffusivity rises. It is noted from the Tables 3 and 4 that the peak temperatures of the peak regions C and D in 1441 alloy are at lower range compared to the those peak temperatures in the 8090 alloy. This implies that the solubility temperatures for the precipitations and dissolutions reactions are at the lower temperature range in the 1441 alloy compared to that in the 8090 alloy.

The peak temperatures of the peak regions for all the exothermic and endothermic reactions have shifted to higher temperatures with increasing heating rates. This implies that the precipitation and dissolution reactions are thermally activated and kinetically controlled [13, 26, 28, 44]. It is reported in literature [26, 29] that in addition to the shifting of peak regions to higher temperatures, the heat effect (heat evolution or heat absorption) of the corresponding peak regions decreases considerably with the increase of heating rate of the DSC run. This is stated to be the fact that the decrease of the solubility of the alloying elements with temperature, causing the amount of phase that can precipitate to decrease with increasing heating rate. In our observation, the heat effects (i.e. the heat evolution or heat absorption) of the different precipitation and dissolution reactions do not vary so much with the heating rates. This is in agreement with the observation of Luo et al. [24].

DSC thermograms of T8, retrogressed (R), RRA and T7 tempers

Figure 6a–f exhibits DSC thermograms of the 8090 alloy in the conventional peak aged (T8), retrogressed at 280 °C (8090R280), retrogressed and under aged (8090R280UA), retrogressed and isothermal peak aged (8090R280IA) and duplex peak aged (8090R280DA) (T77), and over aged (T7) tempers, respectively.

Figure 7a–f shows the DSC thermograms of the 1441 alloy in the peak aged (T8), retrogressed at 230 °C (1441R230), retrogressed and under aged (1441R230UA), retrogressed and isothermal peak

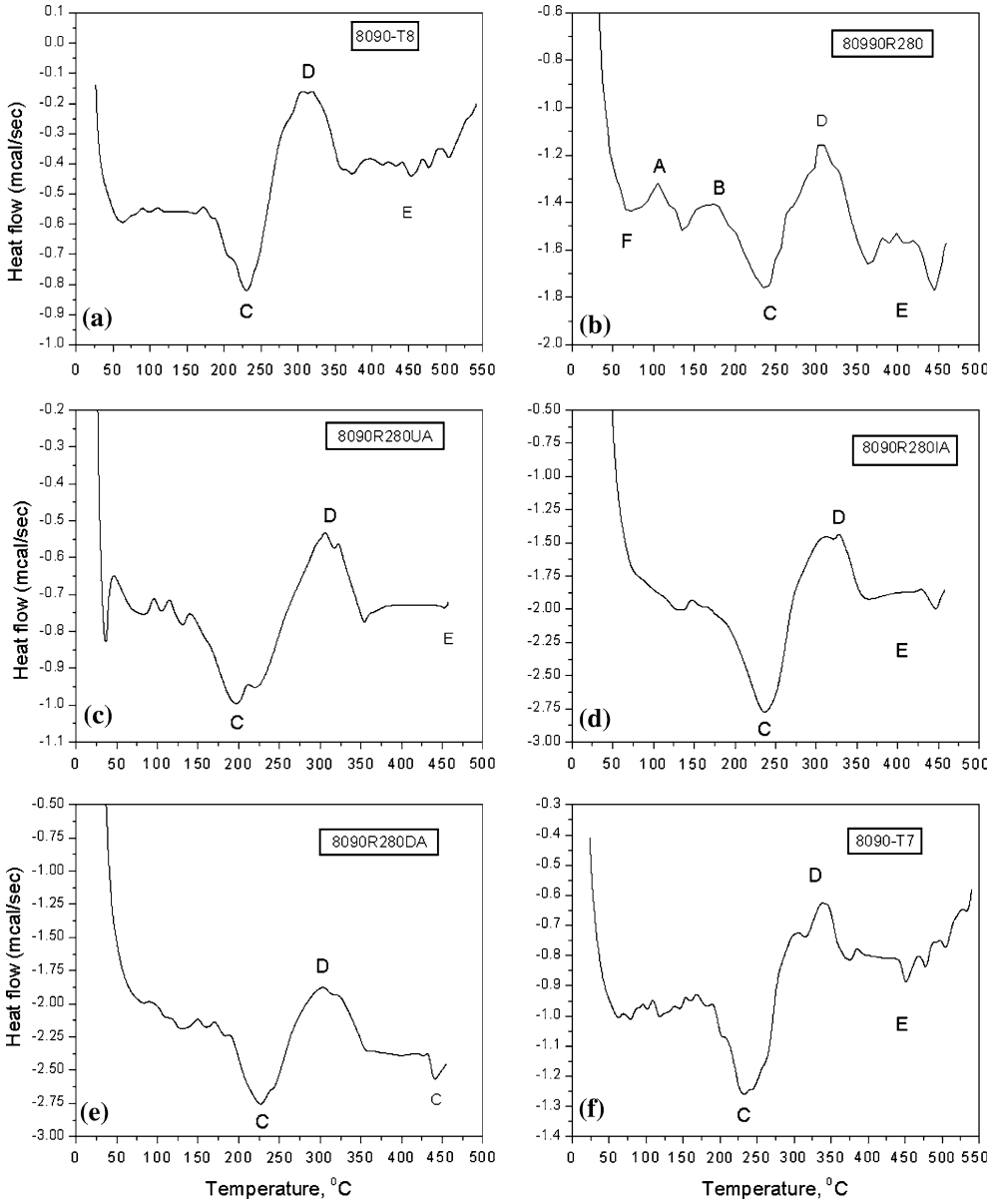

Fig. 6 DSC thermograms of (**a**) 8090-T8, (**b**) 8090R280, (**c**) 8090R280UA, (**d**) 8090R280IA, (**e**) 8090R280DA and (**f**) 8090-T7 at a heating rate of 10 °C/min. The heat effects and peak temperatures of the various peaks are given in Table 5

aged (1441R230IA), retrogressed and duplex peak aged (1441R230DA) (T77), and over aged (T7) tempers, respectively. The heat effects and the peak temperatures of different peak regions associated with different reactions for various tempers of the 8090 and 1441 alloys are given in Tables 5 and 6, respectively.

The thermograms of the peak aged, retrogressed and isothermal and duplex reaged, and over aged tempers for both the alloys (i.e. Figs. 6a, d–f, and 7a, d–f) have two clear endothermic peaks C and E, one exothermic peak region D and thermal fluctuations at low temperature peak regions A and B. The absence and/or less prominent or minutely resolved low temperature exotherms i.e. peak A and peak B in the peak aged tempers implies that the solid solution is not supersatutared with solutes Li, Cu and Mg atoms, but has equilibrium solutes content and the alloy tempers already contain equilibrium amounts of δ' precipitates in the matrix, as seen in Fig. 3a, b, TEM micrographs of the 8090-T8 and 8090R280IA RRA tempers and in Fig. 8a–c, TEM micrographs of the 1441-T8, 1441R270IA and 1441R270DA RRA tempers. But, the low temperature exotherms i.e. peaks A and B, have reappeared in the retrogressed (8090R280 and 1441R230) and in the retrogressed and under aged

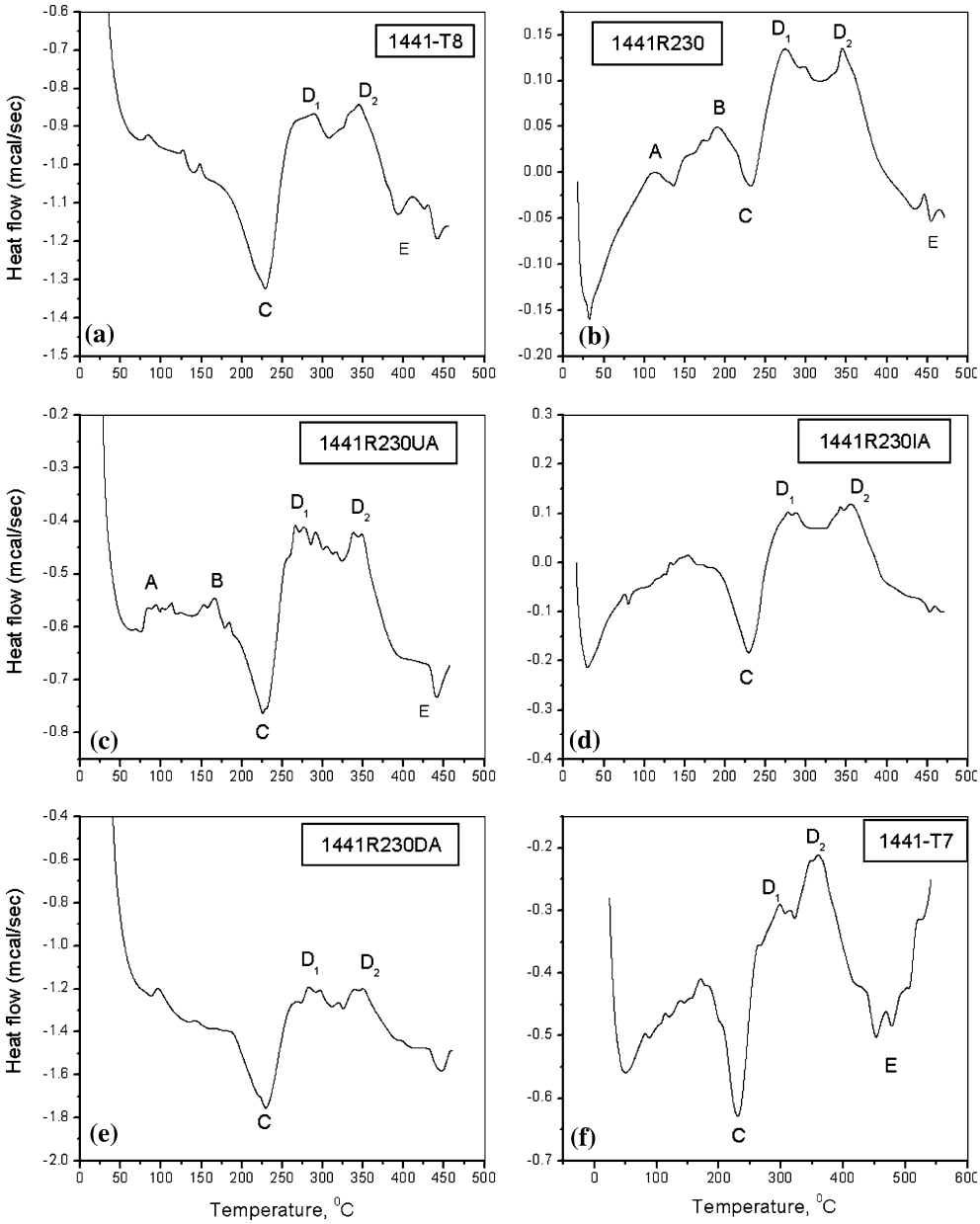

Fig. 7 DSC thermograms of (**a**) 1441-T8, (**b**) 1441R230, (**c**) 1441R230UA, (**d**) 1441R230IA, (**e**) 1441R230DA and (**f**) 1441-T7 at a heating rate of 10 °C/min. The heat effects and peak temperatures of the various peaks are given in Table 6

(8090R280UA and 1441R230UA) tempers in both the alloys. In the retrogressed (R), and retrogressed and under aged (RUA) tempers, the solid solution again is supersaturated with solutes of mostly Li, and a small amounts of Mg and Cu atoms due to the dissolution of δ' and precursors of S′ phases, respectively into the solid solution during retrogression process. So, during DSC runs of the retrogressed state, the reappearance of the peak A (formation of GPB zones) and peak B (precipitation of δ' phase) is obvious. TEM studies were also carried out of the alloys of retrogressed states, but δ' phase could not be detected.

Tables 5 and 6 indicate the heat evolution is less in the RUA tempers compared to that with the retrogressed tempers. This implies that the extent of δ' phase precipitation during DSC run of the RUA tempers is less, as certain amounts of δ' precipitates do already exist in the RUA tempers. So, the driving forces for the formation of GPB zones and δ' precipitation is low in the RUA tempers compared to the tendency for the formations of GPB zones and δ' precipitation in the retrogressed tempers.

For the 1441 alloy in the retrogressed (1441R230) and RUA (1441R230UA) tempers (Fig. 7b, c) the

Table 5 The heat effects associated with the DSC peaks of the 8090 alloy of various tempers

Peak region	Temper					
	8090-T8		8090-T6		8090R280	
	H (mcal/mol)	T_p (°C)	H (mcal/mol)	T_p (°C)	H (mcal/mol)	T_p (°C)
A	–0.05	111	–0.03	112	–0.44	109
B	–0.09	174	–0.10	167	–0.69	184
C	1.70	225	1.50	234	1.08	237
D	–2.59	304, 319	–2.00	305	–1.68	303
E	4.63	372, 453, 477, 505	–	–	–	–
F	0.14	60	0.22	46	0.18	67
	8090R280UA		8090R280IA		8090R280DA	
	H (mcal/mol)	T_p (°C)	H (mcal/mol)	T_p (°C)	H (mcal/mol)	T_p (°C)
A	–0.20	95	–	–	–	–
B	–0.16	139	–	–	–	–
C	1.30	217	1.78	238	1.74	242
D	–2.72	307, 323	3.75	308, 329	–2.21	305, 325
	8090-T7					
	H (mcal/mol)	T_p (°C)				
A	–0.27	97, 110				
B	–0.17	153, 168				
C	1.9	245				
D	–2.20	307, 336, 349				
E	4.25	378, 451, 478, 505				
F	0.26	60				

Table 6 The heat effects associated with the DSC peaks of the 1441 alloy of various tempers

Peak region	Temper					
	1441-T8		1441-T6		1441R230	
	H (mcal/mol)	T_p (°C)	H (mcal/mol)	T_p, °C	H (mcal/mol)	T_p (°C)
A	–0.05	82	–	–	–0.18	122
B	–0.03	148	–0.39	158	–0.19	188
C	1.02	230	1.30	226	0.57	234
D	–3.44	289, 345	–1.74	302	–3.00	283, 345
E	–	–	3.58	451, 468, 503	–	–
F	–	–	0.25	38	0.42	33
	1441R230UA		1441R230IA		1441R230DA	
	H (mcal/mol)	T_p (°C)	H (mcal/mol)	T_p (°C)	H (mcal/mol)	T_p (°C)
A	–0.08	83	–0.03	75	–0.05	95
B	–0.11	183	–0.08	158	–0.02	143
C	0.97	224, 231	1.25	230	1.45	231
D	–4.26	266, 338	–3.85	282, 354	–4.00	284, 351
F	0.18	54	0.24	33	–	
	1441-T7					
	H (mcal/mol)	T_p (°C)				
A	–0.03	81, 113				
B	–0.12	171				
C	0.65	231				
D	–3.27	298, 359				
E	2.73	454, 478				
F	0.42	48				

peak B associated with the precipitation of δ' phase does not overlap with the peak A of GPB zones formation as observed in Figs. 2 and 5. In the retrogression temper, the solid solution is supersaturated with mostly Li and a small amount of Mg and Cu, whereas in the water quenched state the solid solution is supersaturated with solutes of Cu, Li and Mg. The presence of solutes Cu and Mg has an influence on

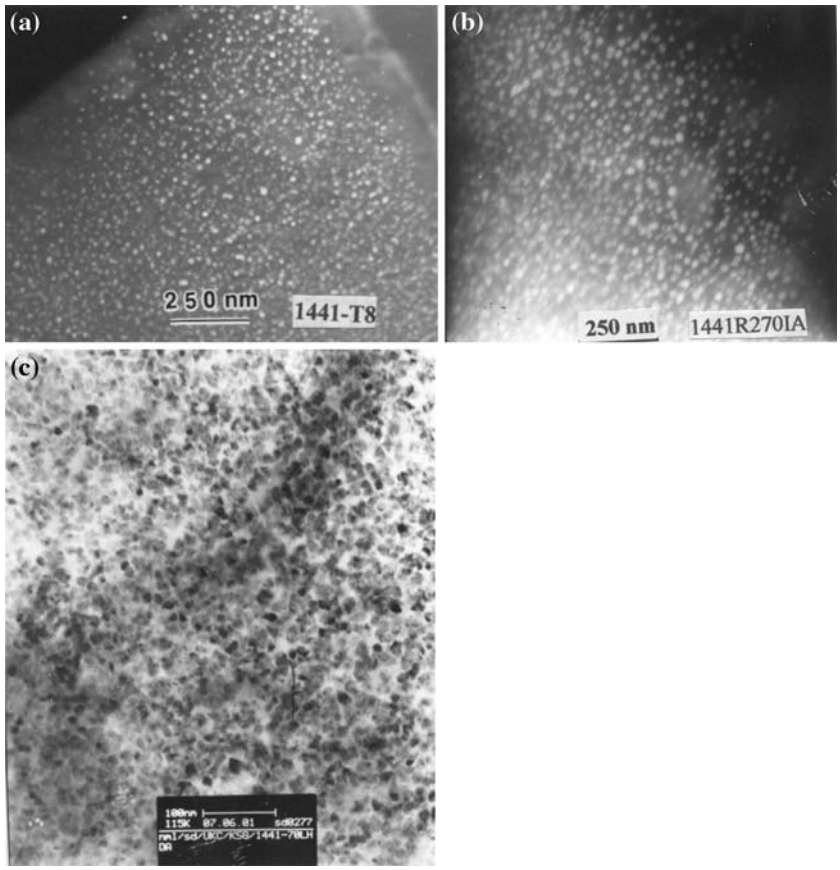

Fig. 8 Dark field images of δ' precipitates in the matrix of (**a**) 1441-T8 and (**b**) 1441R270IA tempers and (**c**) bright field image of δ' precipitates of the 1441R270DA temper

the precipitation of δ' phase at the lower range of temperature and the specific roles are discussed earlier in this section. In the retrogressed and RUA tempers, mostly Li and a small amounts of Cu and Mg atoms being in solid solution, require higher thermal energy for the δ' precipitation compared to that required in water quenched temper. Therefore, the precipitation of δ' in the retrogressed and RUA tempers will occur at higher temperature than the temperature of δ' precipitation in the water quenched state. Hence, in the retrogressed and RUA, there are separate peak regions A and B, and the peak temperature (T_p) of δ' precipitation is at higher temperature as well. Starink et al. [28] mentioned that the growth of the δ' phase is assisted by dislocations, thus the varied amount of dislocations in water quenched temper and in the retrogressed tempers also have some influence in the peak temperature for the δ' precipitation phenomenon. It is interesting to mention, from the DSC thermogram of the retrogressed state (Fig. 7b, exhibiting clearly separate peaks of GPB-zone formation and δ' precipitation) that both phases (GPB zones and δ' precipitates) would definitely form and exist in the 1441 alloy system, which is not a clear indication (due to overlapping peaks at lower temperature) from the DSC thermogram of solution treated and water quenched state of the 1441 alloy (Figs. 2 and 5), arising doubts how strength properties would meet in the alloy.

In the peak region D for the 8090 alloy, peak broadening has taken place, in all the tempers (Fig. 6) except for the water quenched temper (Fig. 1). This indicates that the amount of S′ (S), T_1 and T_2 precipitates is more in the samples which have been subjected to themomechanical treatment after quenching and before artificial aging. The dislocations and defects introduced during thermo-mechanical treatment (TMT) act as sites for the formation of S′ (S), T_1 and T_2 precipitates. In fact, for complete precipitation of S′ (S), T_1 and T_2 phases, thermo-mechanical treatment is required in the 8090 alloy [1, 6, 45, 46].

In the 8090 and 1441 Al–Li–Cu–Mg–Zr alloys, the relative proportions of S′ and T_1 phases are also critically dependent on the relative concentrations of all three main Li, Cu and Mg alloying elements. Magnesium contents above 0.5 wt% ensures a dominance of S′ in alloys containing up to 2.7% lithium and 1.4% copper [6]. Hence, in the 8090 type of alloy, there is a dominance of S′ phase with respect to the T_1. However, with high copper and lithium contents relative to magnesium there is a dominance of T_1 phase. In this context, it may be mentioned that in contrast to T_1,

heterogeneities in the S′ distribution is not manifested in the δ' distribution as the phases precipitates independently. In our present studies, the 1441 alloy containing higher amounts of copper and lower amounts of lithium with respect to that in the 8090 alloy, more amounts of T_1 and T_2 phases are expected in the former alloy. This is exhibited in the DSC thermograms of the 1441 alloy of T8 and RRA tempers which is discussed in the next paragraph.

For the 1441 alloy, in the peak region D, two distinct peaks (i.e., D_1 and D_2) are seen, in all the tempers, (Fig. 7a–f), except for the solution treated and water quenched (Fig. 2). For the alloy 1441, peak D_1 and peak D_2 are clearly revealed, but for the alloy 8090, doublets with separate peak temperatures are not clearly resolved. This implies that the precipitation sequence of S′ (S), T_1, T_2 and δ phases differs in these two alloys. The precipitation sequence is affected by all three alloying elements namely Li, Cu and Mg, as discussed in the earlier.

In 1441 alloy, the peak D_1 region is attributed to the formation of S′ (S) phase whereas the peak D_2 is due to the formation of T_1, T_2 and δ phases [23, 36, 47]. The 1441 alloy has more Cu and less Li compared to the 8090 alloy, so the formation and growth of T_1 and T_2 phases will continue with the DSC run, resulting in separate peak D_2. DSC thermograms of the over aged T7 tempers (Figs. 6f and 7f), show that the D_2 peaks are of greater intensity (increased magnitude) compared to all other tempers. This is attributed to the fact that the DSC traces for the samples of longer aging times indicate the formation of more amounts of T_1, T_2 and equilibrium δ phases.

XRD of T8, retrogressed, RRA and T7 tempers

Figure 9a and b show the diffractograms of the 8090 and 1441 alloys of T8, retrogressed and RRA tempers using CoK_α and CuK_α radiations, respectively. The diffractograms of the T8 and RRA tempers of the alloys, show the peaks of all the probable phases that would be present in the alloy system. But, the diffractograms of the samples, retrogressed at 280 °C for 4 min (Fig. 9a) of the 8090 alloy and retrogressed at 230 °C for 15 min (Fig. 9b) of the 1441 alloy, exhibit the disappearance of $\delta'_{(100)}$ peak and appearance of $T_{1(102)}$ peak. The disappearance of $\delta'_{(100)}$ peak is obvious, and which is attributed to the fact that retrogression has caused dissolution of δ' phase in the solid solution. Further, the appearance of additional $T_{1(102)}$ peak and other intensified peaks of the T_1 and δ phases is due to fact that as δ' phase dissolves into solution during retrogression, the lithium content of the solid solution increases resulting the nucleation and growth of the Li-bearing phases such as T_1, T_2 and δ. The diffractograms of the retrogressed and reaged to peak aged tempers for both the alloys (Fig. 9a and b), show the reappearance of the $\delta'_{(100)}$ peak which is quite obvious because reaging the retrogressed state has resulted in the reprecipitation of δ' phase in the matrix. Therefore, the XRD studies confirm that retrogression of the T8 temper causes dissolution of δ' phase with an attending increase of Li-bearing phases and reaging the retrogressed state causes reprecipitation of δ' phase into matrix.

DSC thermograms of T6 temper

Figure 10a and b show the DSC thermograms of the 8090 and 1441 alloys, respectively, in their peak aged T6 temper. The precipitation sequence is similar to that of the T8 and retrogressed and peak aged tempers. But, there are no such doublets or thermal fluctuations in the peak region D as compared to those observed in the thermograms of peak aged tempers (Figs. 6 and 7). Also, the total heat evolution (Tables 5 and 6) in this peak region D for the T6 temper is less compared to that of the T8 tempers. Thus, this is an evidence of the formation of less amounts of S′ (S), T_1, T_2 and δ precipitates in the T6 tempers. This is obvious and is attributed to the fact that there are very little heterogeneous precipitations of these phases, and instead homogeneous precipitation will be a dominating factor.

The precipitation of S′ and T_1 is greatly favoured by the presence of defects such as dislocations. A thermomechanical treatment which introduces defects such as dislocations and vacancies, is generally required for complete precipitation of S′ and T_1. The presence of dislocations favours heterogeneous precipitation, which requires less supply of thermal energy than that required in homogeneous precipitation. The supply of thermal energy, the release of thermal vacancies (which has formed during quenching) while heating during the DSC run, and the tendency of retaining vacancies (i.e. a counteract of releasing of vacancies) due to strong interaction between Li atoms and vacancies, are not sufficient for the completion of S′ and T_1 precipitation. Therefore, as the as-quenched and the T6 tempers have not been subjected to thermomechanical treatment, no doublets or thermal fluctuitions are observed, instead, a sharp peak is exhibited. If some flattening is observed in the peak region D, this might have arisen due to the formation of more T_1 or S′ on the dislocation sites introduced while punching the DSC samples [28].

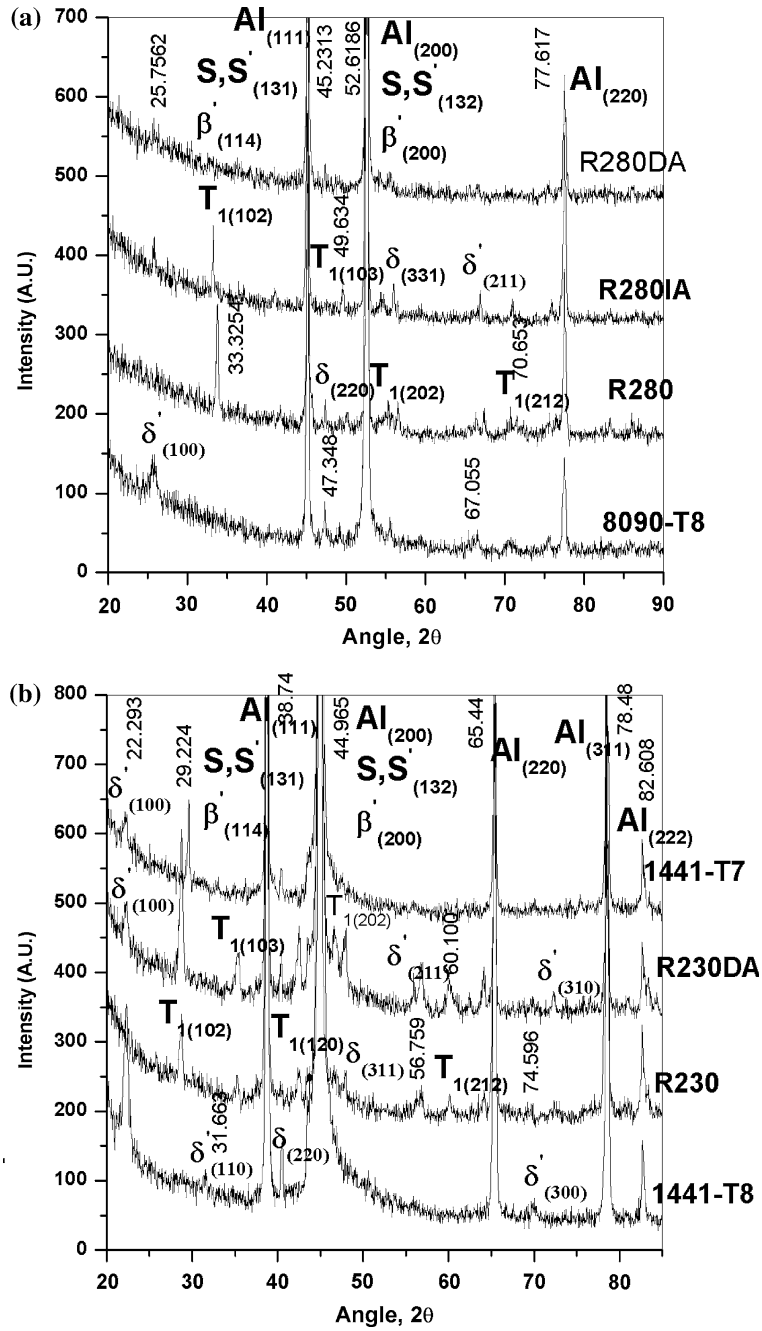

Fig. 9 (**a**) XRD of the 8090 alloy of various tempers using CoK_α radiation, (**b**) XRD of the 1441 alloy of various tempers using CuK_α radiation

Conclusions

DSC thermograms of solution treated and water quenched 8090 and 1441 alloys exhibit many exothermic and endothermic peaks indicating the sequence of precipitation and dissolution reactions of formation of GPB zones, dissolution of Li-lean or order Li-rich regions, precipitation of δ' phase, dissolution of GPB zones and δ' phase, precipitation of S′, T_1, T_2 and δ phases and dissolution of all these phases at higher temperature.

DSC studies of the solution treated and water quenched 8090 and 1441 alloys at different heating rates have indicated shifting of all the exothermic and endothermic reaction peaks at higher temperatures and this implies that the precipitation and dissolution reactions are thermally activated and kinetically controlled processes.

Investigation has indicated that the retrogression treatment causes primarily dissolution of δ' phase into solid solution and reaging the retrogressed states has caused in reprecipitation of δ' phase. This observation

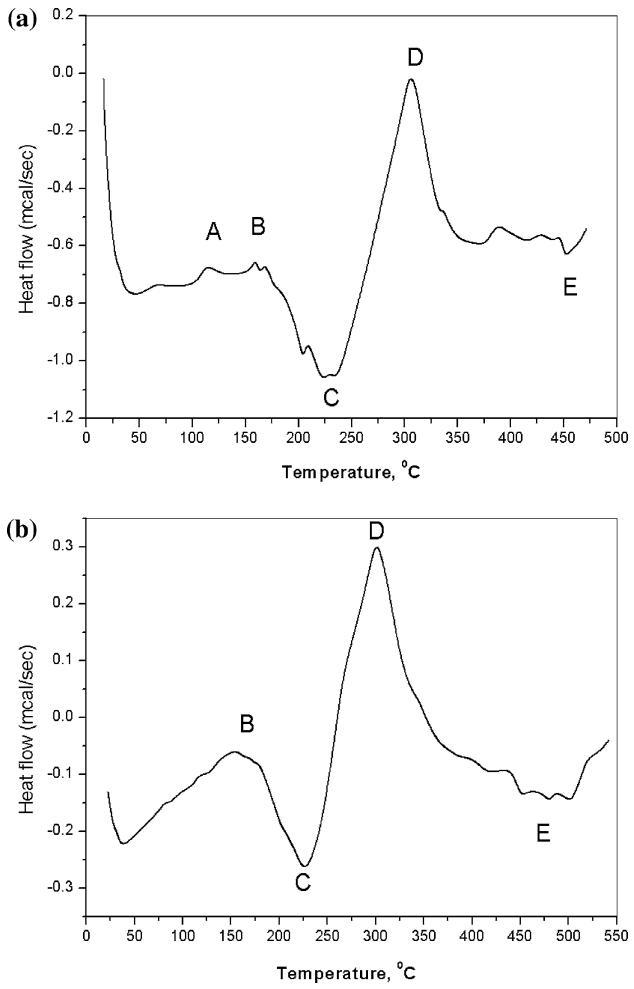

Fig. 10 (**a**) DSC curve of the 8090-T6 temper at a heating rate 10 °C/min, (**b**) DSC curve of the 1441-T6 temper at a heating rate 10 °C/min

has also been confirmed by XRD and TEM studies. Further, the results show that the T8 tempers contain higher amounts of S′, T_1 and T_2 phases compared to that of the T6 tempers, and T7 tempers contain more amounts of equilibrium δ phase.

Thermograms of the retrogressed state of the 1441 alloy showing separate peaks of GPB zones formation and δ' precipitation (as compared to the overlapping peaks of these reactions in the water quenched state) will enable to determine activation energy and growth parameters for these reactions by varying heating rate method.

Acknowledgements The authors would like to thank Mr. Samar Das, National Metallurgical Laboratory, Jamshedpur for TEM studies and Mr. Nirmal Das, Central Research Facility, Indian Institute of Technology, Kharagpur, India for carrying out DSC runs. The authors also thank to Prof. M. Hanumantha Rao, Professor and Dean (Academic) of National Institute of Technology, Warangal, India and Prof. M. J. Starink, Professor of University of Southampton for their valuable technical suggestions.

References

1. Davis JR (ed) (1998) ASM specialty handbook: aluminium lithium alloys. International Materials Information Society, Materials Park, OH, p 121
2. Harris SJ, Noble B, Dinsdale K (1983) In: Sanders TH Jr, Starke EA Jr (eds) Proceeding of the 2nd international conference on aluminium lithium alloys, Warrendale, PA, 1983. TMS and AIME, Warrendale, PA, p 219
3. Christodoulou L, Struble L, Pickens JR (1983) In: Sanders TH Jr, Starke EA Jr (eds) Proceeding of the 2nd international conference on aluminium lithium alloys, Warrendale, PA, 1983. TMS and AIME, Warrendale, PA, p 561
4. Holroyd NJH, Gray A, Scamans GM, Hermann R (1986) In: Baker C, Gregson PJ, Harris SJ, Peel CJ (eds) Proceeding of 3rd international conference on aluminium–lithium alloys, University of Oxford, July, 1985. The Institute of Metals, London, p 310
5. Binsfeld F, Habashi M, Galland J, Fidelle JP, Miannay D, Rofidal P (1987) In: Champier G, Dubost B, Miannay D, Sabetay L (eds) Proceeding of 4th international conference on aluminium lithium alloys, Paris, June, 1987 (Journal de Physique, Suppl. C3, 48), p C3:587
6. Miller WS, White J, Lloyd DJ (1987) In: Champier G, Dubost B, Miannay D, Sabetay L (eds) Proceeding of 4th international conference on aluminium lithium alloys, Paris, June, 1987 (Journal de Physique, Suppl. C3, 48), p C3:139
7. Gregson PJ, Flower HM, Tite CNJ, Mukhopadhyay AK (1986) Mat Sci Technol 2:349
8. Flower HM, Gregson PJ (1987) Mater Sci Technol 3:81
9. Kumar KS, Brown SA, Pickens JA (1996) Acta Mater 44:1899
10. Deiasi R, Adler PN (1977) Metall Trans A 8A:117
11. Adler RN, Deiasi R (1977) Metall Trans A 8A:1185
12. Papazian JM (1981) Metall Trans A 12A:269
13. Papazian JM (1982) Metall Trans A 13A:761
14. Papazian JM, Deiasi RN, Adler PN (1980) Metall Trans A 11A:135
15. Abis S, Evangelista E, Mengucci P, Riontino G (1989) In: Sanders TH Jr, Starke EA Jr (eds) Proceeding of 5th international conference on aluminium lithium alloys, Williamsburg, Virginia, March, 1989. Materials and Component Engineering Publications, Birmingham, p 681
16. Cina B (1974) US Patent No. 3856584, December 24, 1974
17. Cina B, Ranish B (1974) Paper No. XXV, Aluminium Industrial Products. ASM, Pittsburg, PA, October 1974
18. Kanno M, Araki I, Cui Q (1994) Mater Sci Technol 10:599
19. Watkinson PC, Martin JW (1994) Mater Charact 33:11
20. Komisarov V, Tlianker M, Cina B (1998) Mater Sci Eng A242:39
21. Ghosh KS, Das K, Chatterjee UK (2004) Mater Sci Technol 20:825
22. Fox S, Flower HM, Mcdarmaid DC (1986) In: Baker C, Gregson PJ, Harris SJ, Peel CJ (eds) Aluminium lithium alloys III, Proceedings of the 3rd international conference on aluminium–lithium alloys, University of Oxford, July, 1985. The Institute of Metals, London, p 263
23. Mukhopadhyay AK, Tite CNJ, Flower HM, Gregson PJ, Sale F (1987) In: Champier G, Dubost B, Miannay D, Sabetay L (eds) Aluminium lithium alloys IV, Proceedings of the 4th international conference on aluminium lithium

alloys, Paris, June, 1987 (Journal de Phyique, Suppl. 48), p C3:439
24. Luo A, Lloyd DJ, Gupta A, Youdelis WV (1993) Acta Metal Mater 41:769
25. Papazian JM (1986) Mater Sci Eng A 76:97
26. Jena AK, Gupta AK, Chaturvedi MC (1989) Acta Metall 37:885
27. De Macedo MC, Avillez RR, Solorzano IG (1994) Scripta Metal 31:1701
28. Starink MJ, Hobson AJ, Gregson PJ (1996) Scripta Metal 11:1711
29. Starink MJ, Gregson PJ (1996) Mater Sci Forum 217–222:673
30. Harwood JJ (1956) In: Robertson WD (ed) Stress corrosion cracking and embrittlement. John Wiley & Sons
31. Jensrud O, Ryum N (1984) Mater Sci Eng 64:229
32. Nozato R, Nakai G (1977) Trans JIM 18:679
33. Balmuth ES (1984) Scripta Metal 18:301
34. Gregson PJ, Flower HW (1984) J Mater Sci Lett 3:829
35. Radmilovic V, Thomas G, Shiflet GJ, Starke EA Jr (1989) Scripta Metal 23:1141
36. Singh V, Mukhopadhyay AK, Prasad KS (1997) Scripta Metal 37:1519
37. Noble B, Trowsdale AJ (1995) Philos Mag 71:1345
38. Sato T, Tanaka N, Takahasi T (1988) Trans Japan Inst Metals 29:17
39. Shaiu BJ, Li HT, Lee HY, Chen H (1990) Metall Trans A 21:1133
40. Osamura K, Okuda H, Tanaka M, Nagao M (1992) In: Chen H, Vasudevan AK (eds) Kinetics of ordering transformation in metals. Warrendale, Pennsylvania, Metallurgical Society of AIME, p 291
41. Khachaturyan AG, Lindsey TF, Morris JW Jr (1988) Metall Trans A 19:249
42. Lendvai J, Wunderlich W, Gudladi HJ (1993) Philos Mag 67:99
43. Del Rio J, Plazaola F, De Diego N (1994) Philos Mag A 69:591
44. Starink MJ, Gregson PJ (1995) Scripta Metal 33:893
45. Peel CS, Evans B, Baker CA, Bennett DA, Gregson PJ, Flower HM (1983) In: Sanders TH Jr, Starke EA Jr (eds) Proceeding of the 2nd international conference on aluminium lithium alloys, Warrendale, PA, 1983. TMS and AIME, Warrendale, PA, p 363
46. Gregson PJ, Flower HW (1985) Acta Metall 33:527
47. Ozbilen S, Flower HM (1989) In: Sanders TH Jr, Starke EA Jr (eds) Proceeding of 5th international conference on aluminium lithium alloys, Williamsburg, Virginia, March, 1989. Materials and Component Engineering Publications, Birmingham, p 651